Chalcogen bond activation in cation radical salts of naphthalene *peri*-diselenides with *S* = 5/2 magnetic anions.

Hrudya Pariyacheri Padikkal,[a] Olivier Jeannin,[a] Mathieu Rouzières,[b] Rodolphe Clérac,[b] Ie-Rang Jeon,*[,b] and Marc Fourmigué*[,a]

SUPPLEMENTARY INFORMATION

A) Syntheses and crystal growth

Synthesis of 1,8-dibromo-2,7-dimethoxynaphthalene

Slight modifications of the procedure by Press *et al.*[1] was used. N-bromosuccinimide (1.89 g, 10.6 mmol) was dissolved in 26 ml of chloroform and then treated with pyridine (0.85 ml, 10.6 mmol) after its complete dissolution. The solution was refluxed under argon for 1 h. A solution of 2,7-dimethoxynaphthalene (0.48 g, 2.66 mmol) in 2.9 ml of chloroform was added dropwise and refluxing was continued overnight. The mixture was cooled to room temperature and concentrated. The solid residue was purified by flash column chromatography on silica gel (Petroleum ether: ethyl acetate, 9:1) to afford 1.66 g (56%) of the product as pale yellow crystalline solid. ^{1}H NMR (400 MHz, $CDCl_3$) δ 7.74 (d, *J* = 9.0 Hz, 2 H), 7.16 (d, *J* = 9.0 Hz, 2 H), 4.02 (s, 6 H).

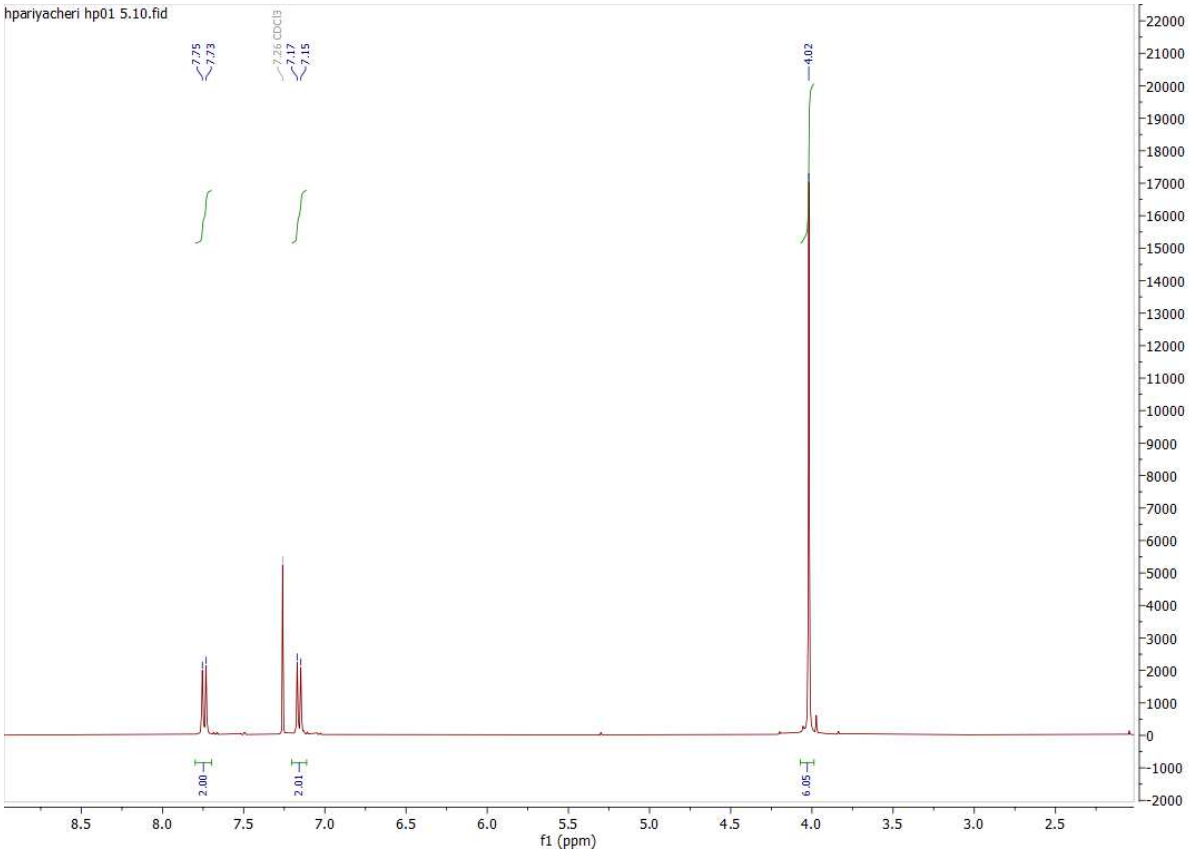

Fig. S1 ^{1}H NMR of 1,8-dibromo-2,7-dimethoxynaphthalene.

Synthesis of 3,8-dimethoxynaphtho[1,8-cd]-1,2-diselenole 1. A solution of 1,8-dibromo-2,7-dimethoxynaphthalene (0.2 g, 0.58 mmol) in 30 ml of dry THF was cooled to -78°C under argon. *n*-Butyllithium (1 ml, 1.6 M, 1.6 mmol) was added dropwise and the mixture was brought to room temperature over 1.5 h. The mixture was then cooled to 0°C, dried elemental selenium (126 mg, 1.6 mmol) was quickly introduced and the argon atmosphere was restored. The mixture was warmed to room temperature and stirred overnight. The reaction mixture was then quenched with saturated ammonium chloride solution (10 ml). Air was rapidly bubbled through the mixture for 30 minutes and the mixture was left in open air. THF was evaporated, CH_2Cl_2 was added and then the mixture was washed with brine, dried over $MgSO_4$, filtered, and concentrated under reduced pressure. The resulting dark violet solid was dissolved in CH_2Cl_2, adsorbed on Celite® and purified by flash column chromatography (Petroleum ether: ethyl acetate, 9:1) to afford 0.15 g (79%) of the compound as purple crystalline solid. ^{1}H NMR (400 MHz, $CDCl_3$) δ 7.56 (d, *J* = 8.8 Hz, 2 H), 6.96 (d, *J* = 8.8 Hz, 2 H), 3.97 (s, 6 H). Elem. Anal. Calcd. for $C_{12}H_{10}O_2Se_2$: C, 41.87; H, 2.93; found: C, 42.87; H, 2.92.

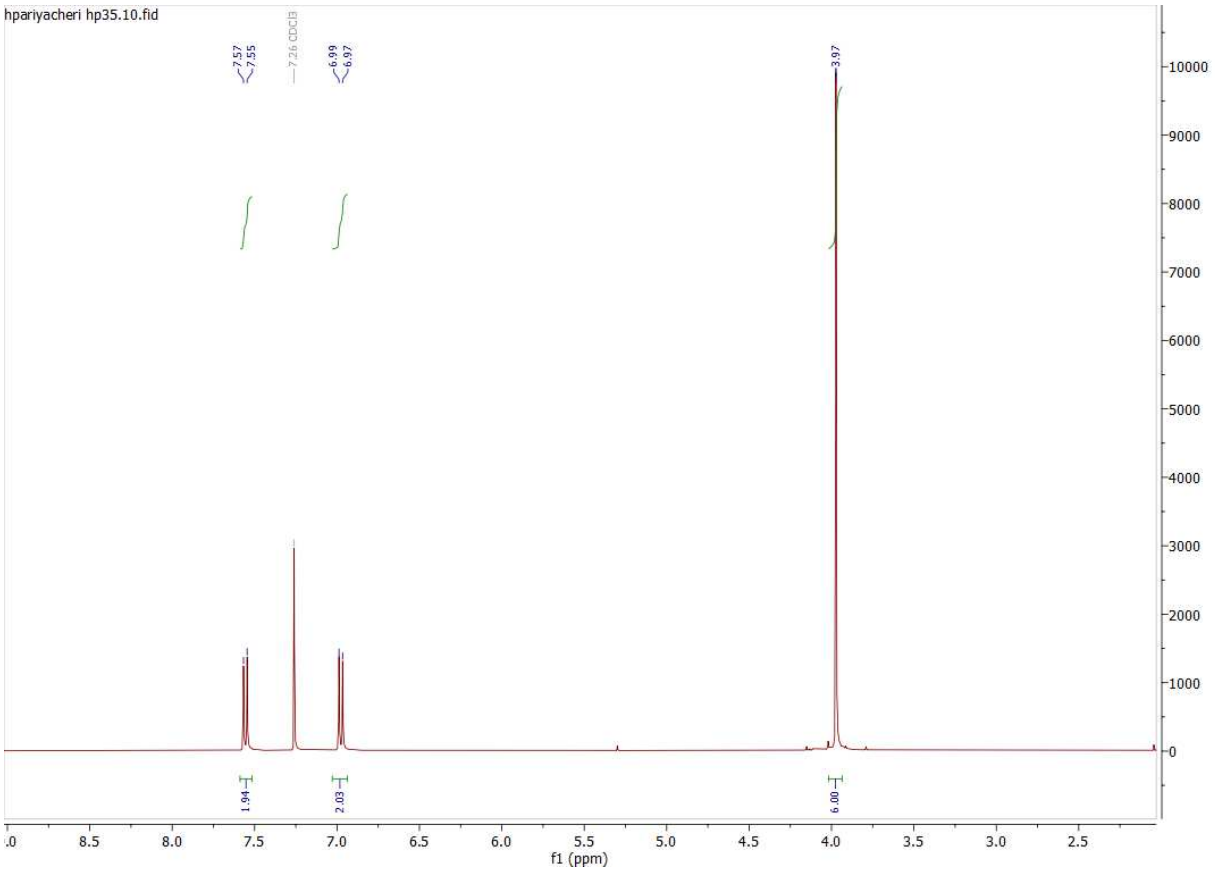

Fig. S2 ^{1}H NMR of 3,8-dimethoxynaphtho[1,8-cd]-1,2-diselenole **1**.

B) Electrocrystallizations

Preparation of the electrolytes

Synthesis of (*n*-Bu_4N)$FeCl_4$.[2] An aqueous solution of (*n*-Bu_4N)OH (12 ml of a 40% solution in water, 22.4 mmol) was added dropwise to a solution of $FeCl_3.H_2O$ (1.816 g, 11.2 mmol) in 200 ml of 8M HCl (aq) under air. A yellow solid precipitated was then filtered. The solid was washed twice with diethyl ether and dried under vacuum. It was then dissolved in dry CH_2Cl_2, Et_2O was added to the solution, and it was cooled to 0 °C overnight. Yellow shiny crystals of the title compound were obtained with a yield of 57% (3.48 g). Elem. Anal. Calcd. for $C_{16}H_{36}NFeCl_4$: C, 43.66; H, 8.24; N, 3.18; found: C, 43.61; H, 8.16; N, 2.98.

Synthesis of (*n*-Bu_4N)$GaCl_4$. Solutions of (*n*-Bu_4N)Cl (1.47 g, 5.3 mmol) and gallium (III) chloride (0.93 g, 5.3 mmol) in 10ml of degassed methanol were mixed together to obtain a white precipitate. This precipitate was then filtered and recrystallised in hot methanol and white shiny crystals of the title compound were obtained with a yield of 54 % (1.3 g). Elem. Anal. Calcd. for $C_{16}H_{36}NGaCl_4$: C, 42.33; H, 7.99; N, 3.09; found: C, 42.60; H, 8.07; N, 2.99.

Synthesis of (*n*-Bu_4N)$FeBr_4$.[3] Solutions of (*n*-Bu_4N)Br (2 g, 6.2 mmol) and iron (III) bromide (1.83 g, 6.2 mmol) in 25 ml of ethanol were mixed together to obtain a brown precipitate. This precipitate was then filtered and recrystallised in hot ethanol and brown shiny crystals of the title compound were obtained with a yield of 68 % (2.36 g). Elem. Anal. Calcd. for $C_{16}H_{36}NFeBr_4$: C, 31.1; H, 5.87; N, 2.27; found: C, 30.86; H, 5.59; N, 1.99.

Synthesis of (*n*-Bu_4N)$GaBr_4$.[3] Solutions of (*n*-Bu_4N)Br (1.04 g, 3.23 mmol) and gallium (III) bromide (1 g, 3.23 mmol) in 25 ml of degassed methanol were mixed together to obtain a white precipitate. This precipitate was then filtered and recrystallised in hot methanol and white shiny crystals of the title compound were obtained with a yield of 55 % (1.12 g). Elem. Anal. Calcd. for $C_{16}H_{36}NFeBr_4$: C, 30.42; H, 5.74; N, 2.22; found: C, 30.27; H, 5.54; N, 2.22.

Electrocrystallization conditions. All salts were obtained from the electrocrystallization of donor molecule **1** (7 mg), using (*n*-Bu_4N)Fe/GaX_4 (100 mg) as electrolyte, in 1,2-dichloroethane (10 mL). Platinum electrodes (length 1.5 cm, diameter 1 mm) were used in a galvanostatic mode with a constant current of 3 μA, at controlled temperature (20 ±2° C).

C) Crystallography

Single crystals of (**1**)(Fe/GaX_4), X = Cl, Br that were suitable for X-ray analysis were coated with Paratone-N oil and mounted on a MicroMountsTM rod. X-ray diffraction measurements were performed on a Bruker APEX II diffractometer operating with a Mo Kα (λ = 0.71073 Å) X-ray tube with a graphite monochromator. Structures were solved by a dual-space algorithm using SHELXT[4] and then refined with full-matrix least-square methods based on F^2 (SHELXL-2014)[5] with the aid of the WINGX program.[6] All non-hydrogen atoms were refined with anisotropic atomic displacement parameters. H atoms were finally included in their calculated positions.

The large residuals densities and low bond precision found in (**1**)($GaCl_4$) may result from a third disorder position (at least) of the $GaCl_4^-$ anion that could not be refined, even with constraints and restrictions on the distances in U_{ij}. This unaccounted disorder affects the residual density as well as the bond precision.

CCDC searches

A search for short halogen-halogen intermolecular contacts between MX_4^- anions was performed based on single crystal structures containing such MX_4^- anions (M = Fe, Ga ; X = Cl, Br) available in the CCDC. The number of hits was 94, 81,12 and 23 with a number of observable values exported for the calculation of average distances of 125, 102, 15, and 26 for $GaCl_4^-$, $FeCl_4^-$, $GaBr_4^-$, and $FeBr_4^-$, respectively. The distance range was 3.555-3.640, 3.170-3.640, 3.406-3.704 and 3.459-3.714 Å for $GaCl_4^-$, $FeCl_4^-$, $GaBr_4^-$, and $FeBr_4^-$, respectively.

Table S1 Crystallographic data.

	(**1**)($FeCl_4$)	(**1**)($GaCl_4$)	(**1**)($GaCl_4$)_B	(**1**)($FeBr_4$)	(**1**)($GaBr_4$)
CCDC	2497447	2497448	2497449	2497450	2497451
Formulae	$C_{12}H_{10}Cl_4FeO_2Se_2$	$C_{12}H_{10}Cl_4GaO_2Se_2$	$C_{12}H_{10}Cl_4GaO_2Se_2$	$C_{12}H_{10}Br_4FeO_2Se_2$	$C_{12}H_{10}Br_4GaO_2Se_2$
FW ($g.mol^{-1}$)	541.77	555.64	555.64	719.61	733.48
System	monoclinic	triclinic	triclinic	monoclinic	monoclinic
Space group	$P2_1/n$	$P\bar{1}$	$P\bar{1}$	$P2_1/n$	$P2_1/n$
a (Å)	6.8876(6)	6.8755(12)	6.8366(8)	6.9157(5)	6.9210(9)
b (Å)	24.250(2)	10.5581(18)	13.2303(15)	24.6933(19)	24.702(3)
c (Å)	10.5956(10)	13.307(2)	19.885(2)	10.9028(7)	10.9454(11)
α (deg)	90.00	109.147(5)	72.788(4)	90.00	90.00
β (deg)	102.284(3)	99.047(5)	87.095(4)	102.701(3)	102.557(5)
γ (deg)	90.00	101.950(6)	84.530(4)	90.00	90.00
V ($Å^3$)	1729.2(3)	865.9(3)	1709.8(3)	1816.3(2)	1826.5(4)
T (K)	150(2)	150(2)	150(2)	150(2)	150(2)
Z	4	2	4	4	4
Cryst. dim. (mm)	0.14×0.05×0.03	0.11×0.05×0.03	0.17×0.07×0.01	0.18×0.05×0.02	0.12×0.05×0.02
D_{calc} ($g.cm^{-3}$)	2.081	2.131	2.159	2.632	2.667
μ (mm^{-1})	5.698	6.408	6.49	13.636	14.241
Absorption corr.	multi-scan	multi-scan	multi-scan	multi-scan	multi-scan
T_{min}, T_{max}	0.718, 0.843	0.688, 0.825	0.586, 0.937	0.446, 0.761	0.430, 0.752
Total refls	23280	18599	42546	20229	4155
Uniq refls (R_{int})	3961 (0.0356)	3973 (0.0842)	7807 (0.0447)	4144 (0.0399)	4155
Uniq refls ($I > 2\sigma(I)$)	3487	3290	6670	3613	3767
R_1, wR_2	0.0242, 0.0463	0.1093, 0.2712	0.0388, 0.0888	0.0307, 0.0661	0.0385, 0.0739
R_1, wR_2 (all data)	0.0302, 0.0479	0.1255, 0.2799	0.0478, 0.0926	0.0376, 0.0682	0.045, 0.0756
GOF	1.089	1.152	1.091	1.092	1.189

D) Theoretical calculations

Geometrical optimizations of the molecules were carried out with density functional theory using the Gaussian 16, Revision C.01 software, the B3LYP functional, the def2TZVP basis set and D3 empirical dispersion correction for all atoms. GaussView 5.0.9 was used to generate the figures. The isovalues, in e/bohr^3, used for the figures are 0.001 for ESP maps, 0.004 for spin density maps and 0.04 for MO's (1 bohr = 1 atomic unit (a.u.) = 0.529177249 Å). The scale used for the ESP maps ranges from –0.035 to +0.015 a.u. for neutral **1** and from 0.1 to 0.13 a.u. for $\mathbf{1}^{+\bullet}$ radical cation.

Table S2 Final coordinates after geometrical optimization for neutral **1**.

C	1.22802309	0.14041001	0.00014600
C	2.42832717	0.82204806	0.00011200
C	2.42914418	2.23375416	0.00003500
C	1.24478809	2.93008321	-0.00000600
C	-0.00001500	2.26289616	0.00002700
C	-1.24482209	2.93007421	-0.00001400
C	-2.42917318	2.23373716	0.00002000
C	-2.42834718	0.82203106	0.00009700
C	-1.22803909	0.14040201	0.00013800
C	-0.00001000	0.83401706	0.00010500
C	4.82489235	0.67751405	0.00016400
C	-4.82491135	0.67748105	0.00002200
O	3.55263826	0.04973400	0.00015300
O	-3.55265226	0.04971000	0.00014300
Se	1.19804508	-1.77488613	0.00024700
Se	-1.19804708	-1.77489513	0.00024200
H	3.36465524	2.77377920	0.00000800
H	1.25913809	4.01299729	-0.00006500
H	-1.25918009	4.01298829	-0.00007200
H	-3.36468824	2.77375620	-0.00001000
H	4.96742036	1.29305110	-0.89312606
H	5.55441840	-0.12900601	0.00022200
H	4.96736436	1.29313009	0.89341007
H	-4.96746736	1.29312310	0.89323606
H	-5.55443242	-0.12904401	0.00004000
H	-4.96736236	1.29299109	-0.89330007

E(rb3lyp) = -5417.176511 hartree, no imaginary frequency

Table S3 Final coordinates after geometrical optimization for $\mathbf{1}^{+\bullet}$ radical cation

C	1.22073309	0.14800801	0.00014400
C	2.44748817	0.83515706	0.00010000
C	2.43861417	2.23989316	0.00002400
C	1.24362209	2.93122121	-0.00001000
C	-0.00001500	2.26810116	0.00003000
C	-1.24365709	2.93121221	-0.00000400
C	-2.43864418	2.23987716	0.00003900
C	-2.44750818	0.83514006	0.00011900
C	-1.22074909	0.14799901	0.00015300
C	-0.00001000	0.84451406	0.00011000
C	4.84686835	0.66338905	0.00016300
C	-4.84688635	0.66335605	0.00000700
O	3.53818526	0.06625500	0.00012800
O	-3.53820025	0.06623100	0.00018000
Se	1.17373208	-1.73382513	0.00024400
Se	-1.17373408	-1.73383313	0.00026100
H	3.37021224	2.78537720	-0.00001200
H	1.25995209	4.01384029	-0.00007200
H	-1.25999309	4.01383129	-0.00006100
H	-3.37024624	2.78535320	0.00001400
H	4.99090936	1.26743709	-0.89683607
H	5.54274941	-0.16951601	0.00023400
H	4.99082336	1.26752209	0.89711806
H	-4.99098036	1.26750409	0.89693006
H	-5.54276242	-0.16955301	-0.00000600
H	-4.99079836	1.26738709	-0.89702307

E(rb3lyp) = -5416.948121 hartree, no imaginary frequency

E) Structural description of (1)(GaCl$_4$)_B phase.

(**1**)(GaCl$_4$)_B phase crystallizes in the triclinic system, space group $P\bar{1}$, with two crystallographically independent radical cations $\mathbf{1}^{+\bullet}$ and two crystallographically independent $GaCl_4^-$ anions. Evolutions of intramolecular bond distances within the two crystallographically independent radical cations $\mathbf{1}^{+\bullet}$ (Cf Table S4) vs. the neutral donor molecule **1** indicate a common +1 charge for both donor molecules.

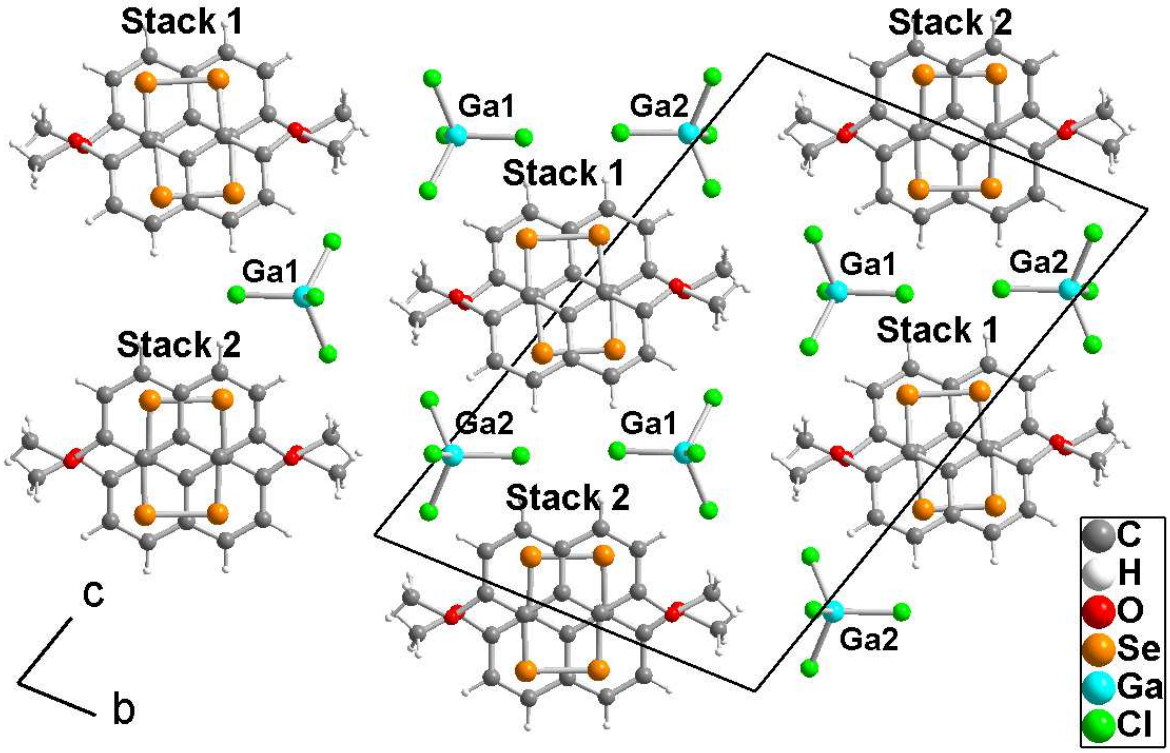

Fig. S3 Projection view along the *a* axis of the unit cell of (**1**)(GaCl$_4$)_B, showing the independent stacks 1 and 2 and the independent $GaCl_4^-$ anions.

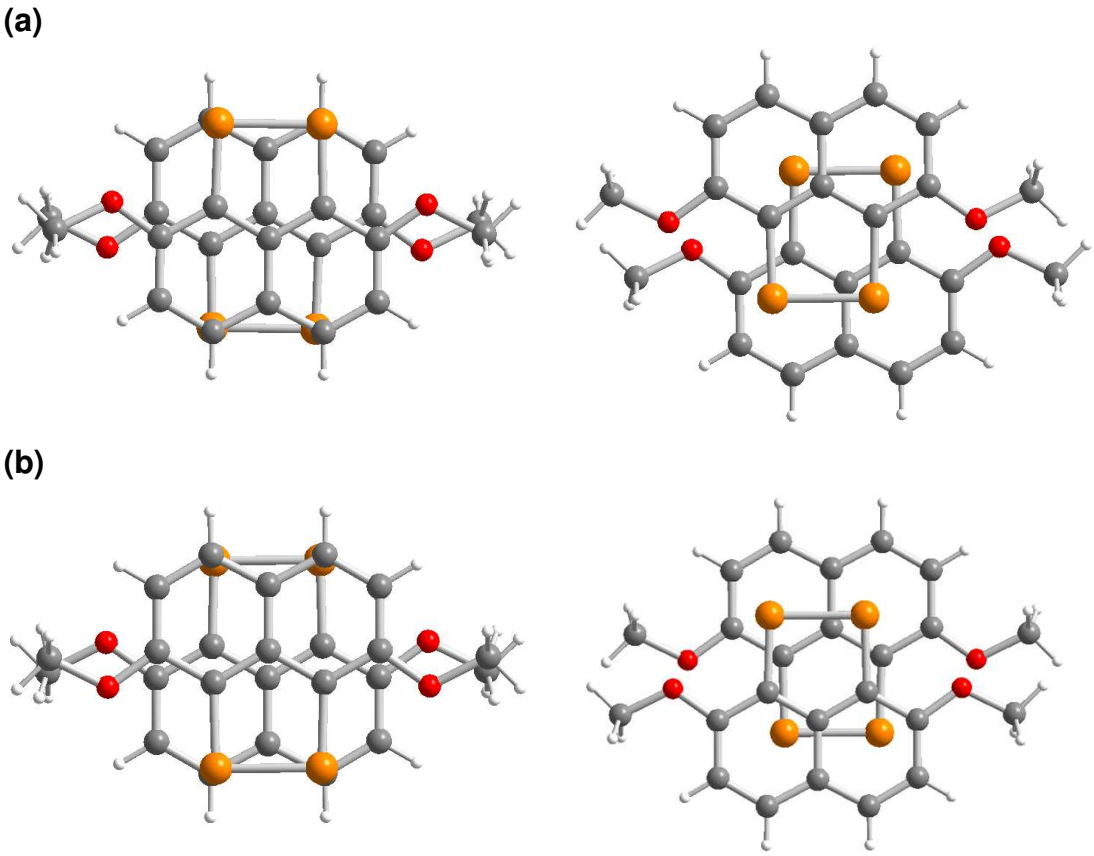

Fig. S4 Overlap interactions in (**1**)($GaCl_4$)_B in (a) stack 1 and in (b) stack 2.

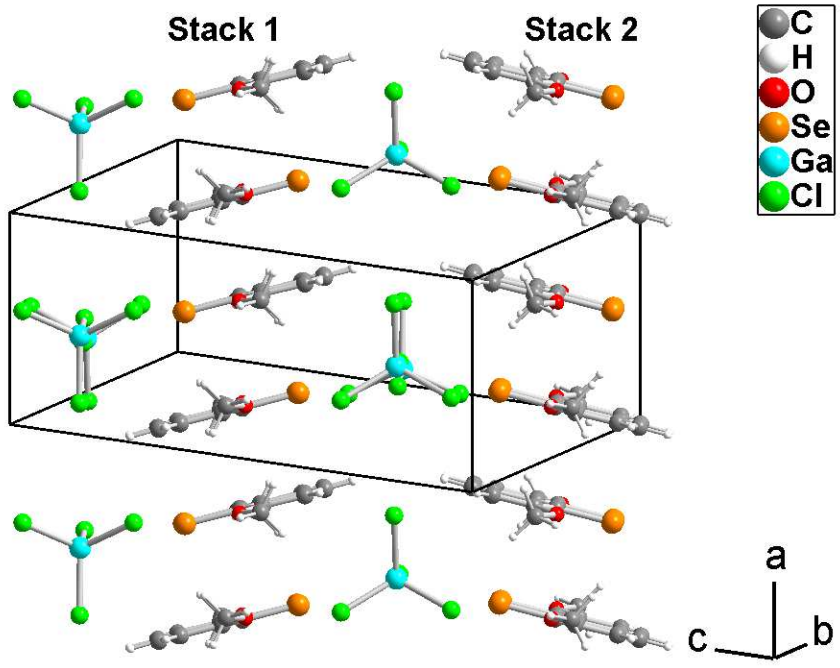

Fig. S5 Relative orientation of the neighboring stacks in (**1**)($GaCl_4$)_B.

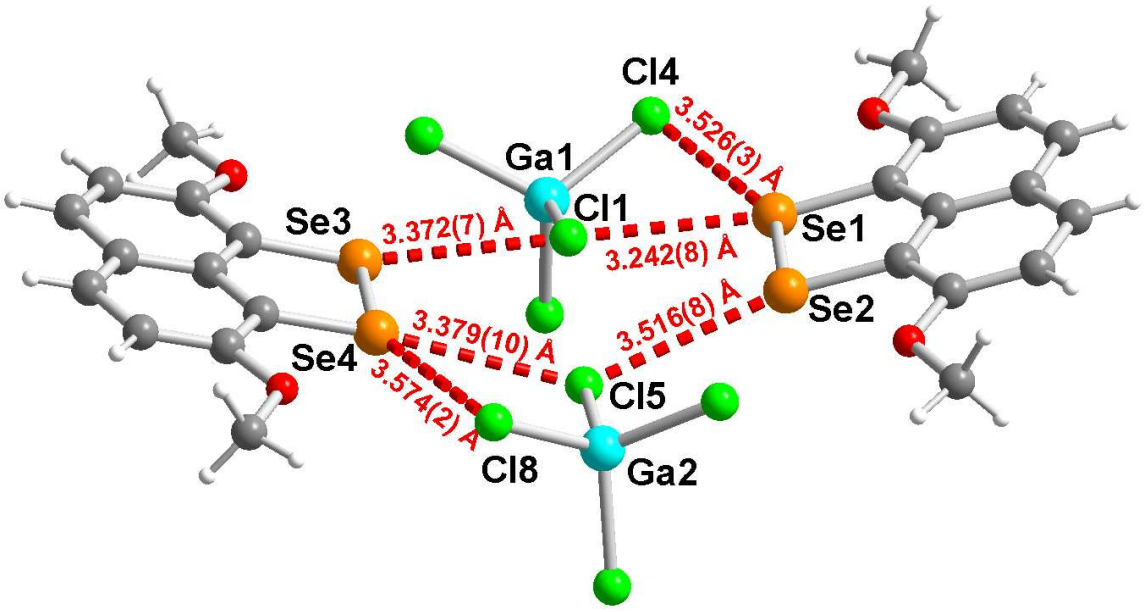

Fig. S6 ChB interactions in (**1**)($GaCl_4$)_B.

Table S4 Evolutions of intramolecular bond lengths in **1**, in neutral and cation radical state.

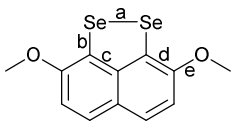

	a	b	c	d	e	ref
Neutral **1**	2.355(4)	1.904(2) 1.903(2)	1.406(3) 1.412(4)	1.371(3) 1.379(3)	1.373(3) 1.373(4)	7
(**1**)($FeCl_4$)	2.322(1)	1.872(3) 1.873(3)	1.402(4) 1.404(3)	1.401(3) 1.406(3)	1.344(3) 1.345(3)	this work
(**1**)($FeBr_4$)	2.322(1)	1.869(4) 1.873(4)	1.400(6) 1.403(5)	1.403(6) 1.407(6)	1.338(5) 1.342(5)	this work
(**1**)($GaCl_4$)	2.323(3)	1.868(6) 1.870(6)	1.396(6) 1.402(6)	1.409(6) 1.411(6)	1.336(5) 1.339(6)	this work
(**1**)($GaCl_4$)_B Mol 1 Mol 2	2.322(3) 2.323(3)	1.865(6) 1.874(6) 1.868(6) 1.870(6)	1.399(6) 1.403(6) 1.396(6) 1.402(6)	1.399(6) 1.409(6) 1.409(7) 1.411(7)	1.345(5) 1.332(6) 1.336(5) 1.339(6)	this work
(**1**)($GaBr_4$)	2.322(1)	1.871(7) 1.876(7)	1.396(7) 1.409(7)	1.409(7) 1.417(7)	1.336(7) 1.346(7)	this work

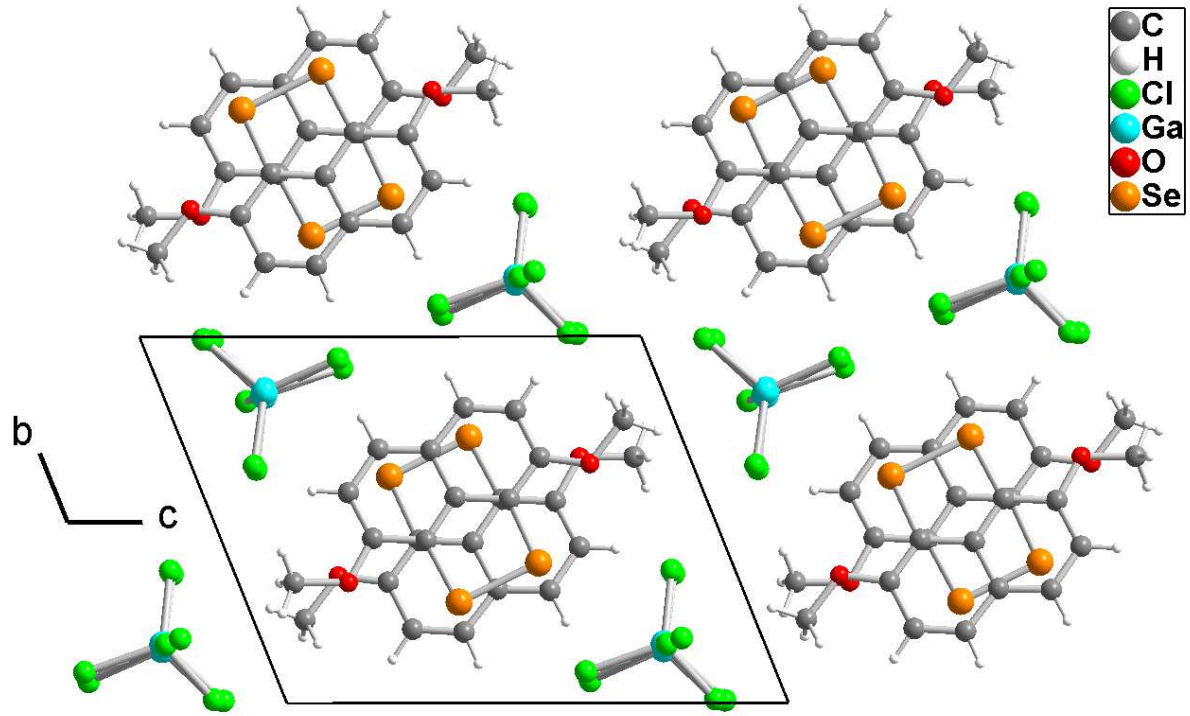

Fig. S7 Projection view along *a* of the unit cell of (**1**)($GaCl_4$).

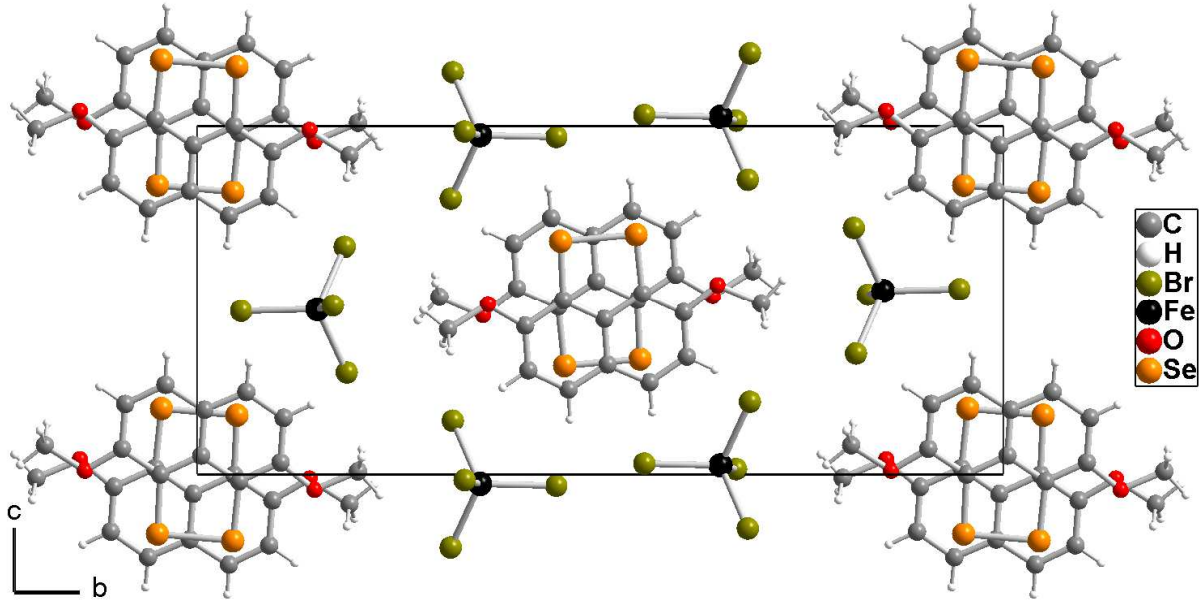

Fig. S8 Projection view along *a* of the unit cell of (**1**)($FeBr_4$).

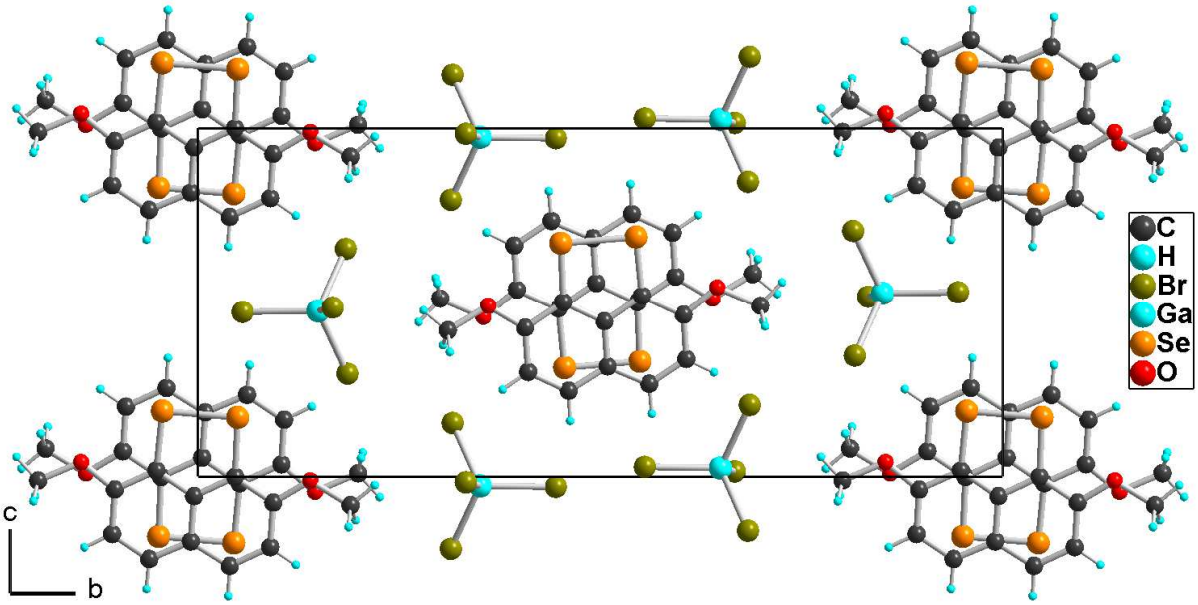

Fig. S9 Projection view along *a* of the unit cell of (**1**)($GaBr_4$).

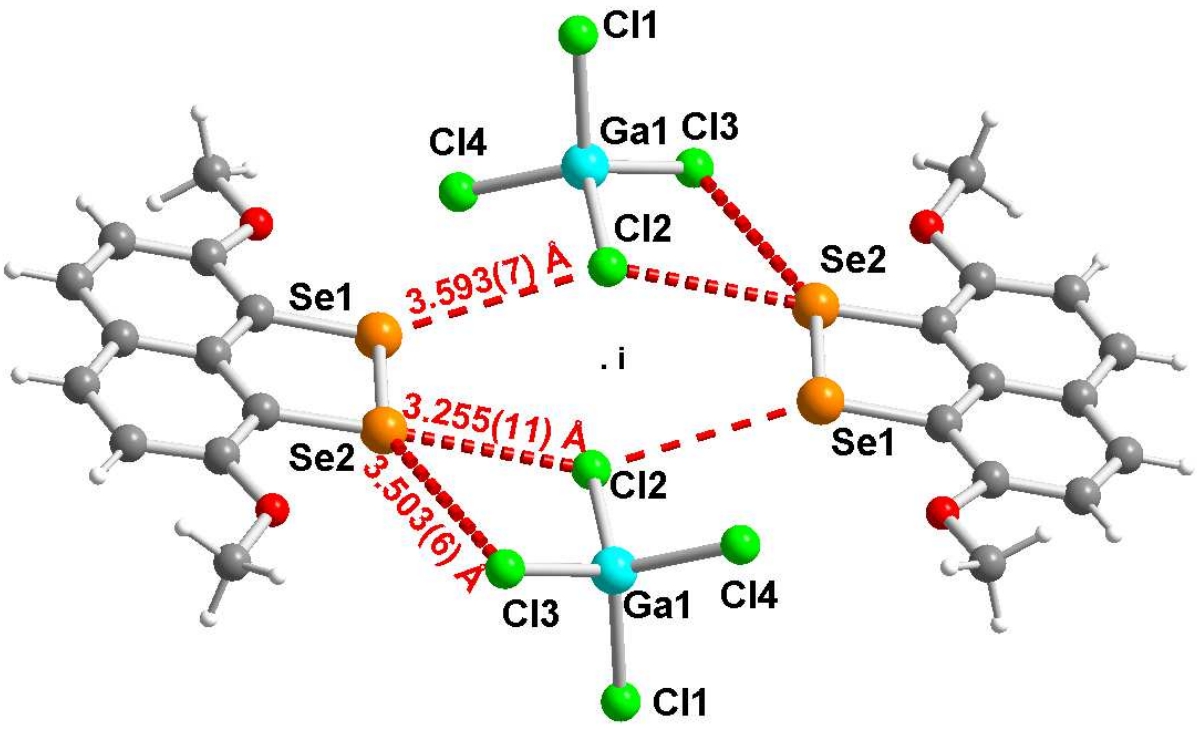

Fig. S10 Detail of the ChB interactions (red dotted lines) in (**1**)($GaCl_4$). Only the major component (91%) of the disordered $GaCl_4^-$ anion is shown.

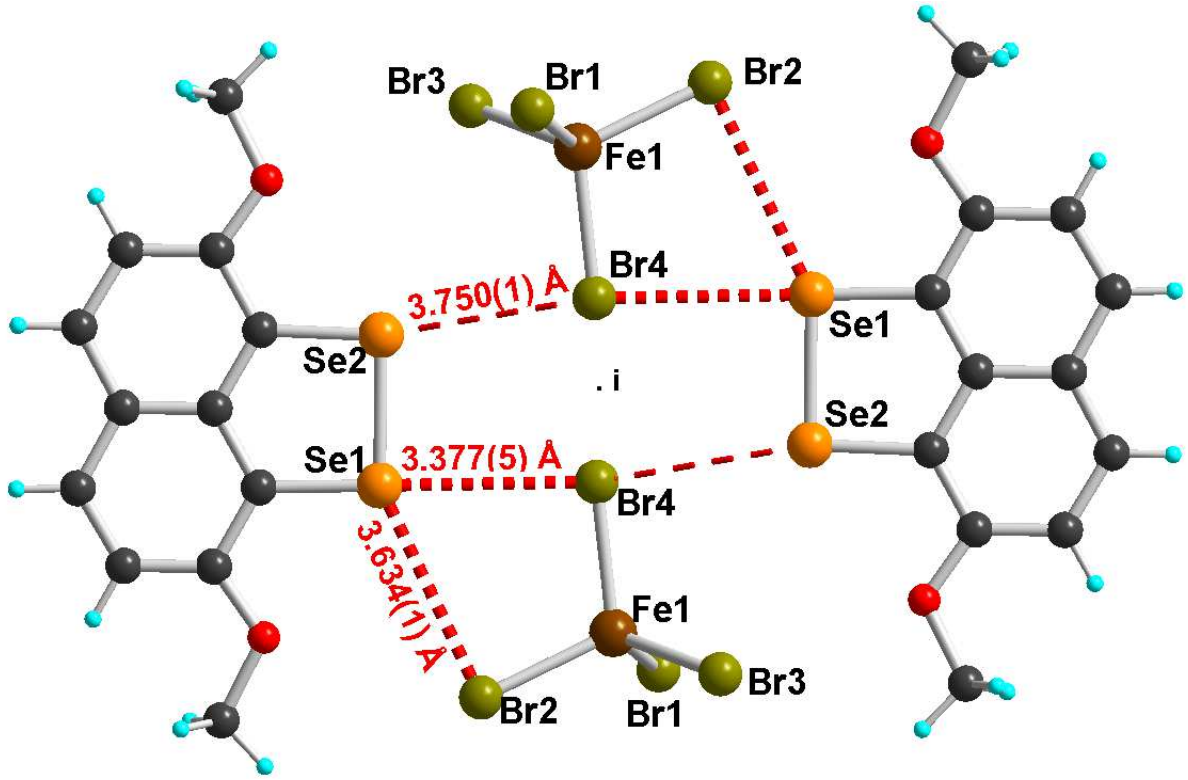

Fig. S11 Detail of the ChB interactions (red dotted lines) in (**1**)($FeBr_4$).

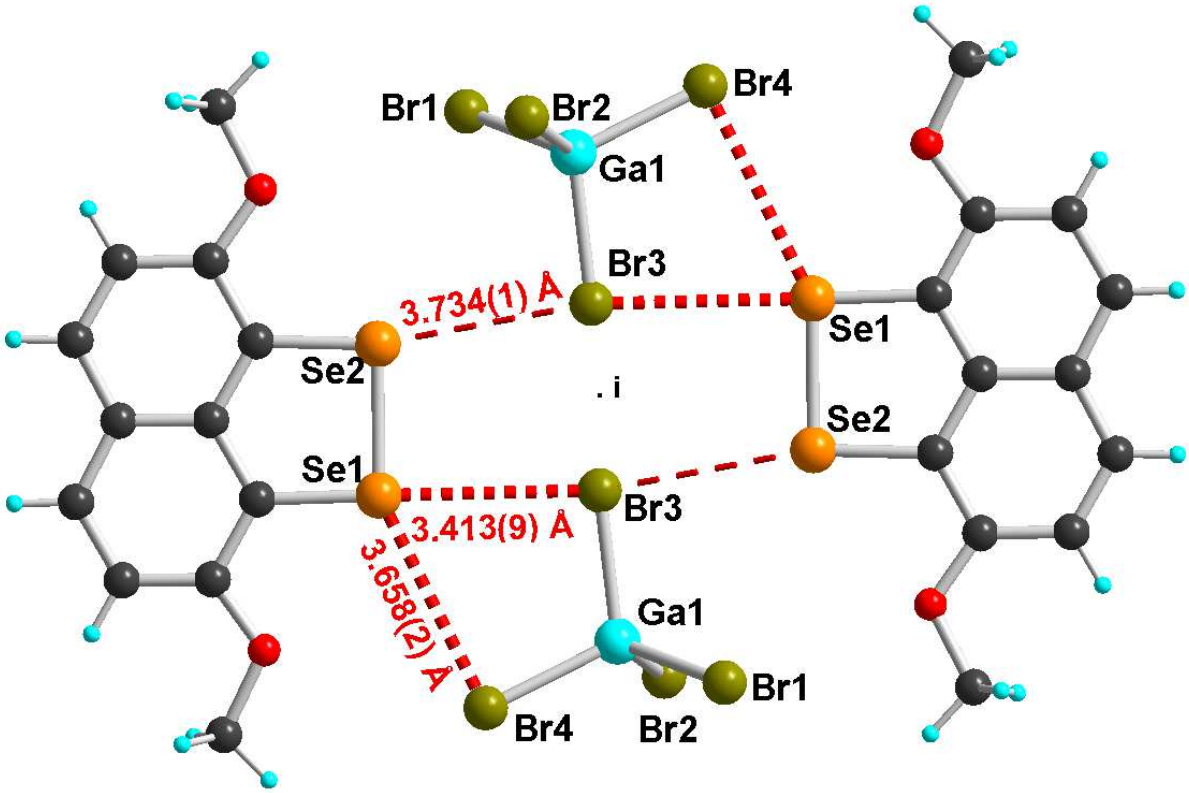

Fig. S12 Detail of the ChB interactions (red dotted lines) in (**1**)($GaBr_4$).

F) Magnetic properties

The magnetic measurements were carried out with a Quantum Design MPMS-XL SQUID magnetometer working between 1.85 and 400 K with applied static fields (H) ranging from –7 to 7 T. The data were collected on polycrystalline samples of (**1**)($FeCl_4$) (9.40 and 9.26 mg) and (**1**)($FeBr_4$) (8.5 and 13.27 mg), sealed in a polypropylene bag (size ≈ 1 × 0.5 × 0.02 cm; 20-23 mg). The resulting data were corrected for the sample holder and intrinsic diamagnetic contributions of the sample. The alternating current (ac) susceptibility measurements down to 1.85 K were performed using an oscillating field of 3 Oe for frequencies (ν_{ac}) between 1 to 1.5 kHz in zero-dc field. In the available temperature and frequency ranges, the samples do not display any observable slow relaxation of the magnetization.

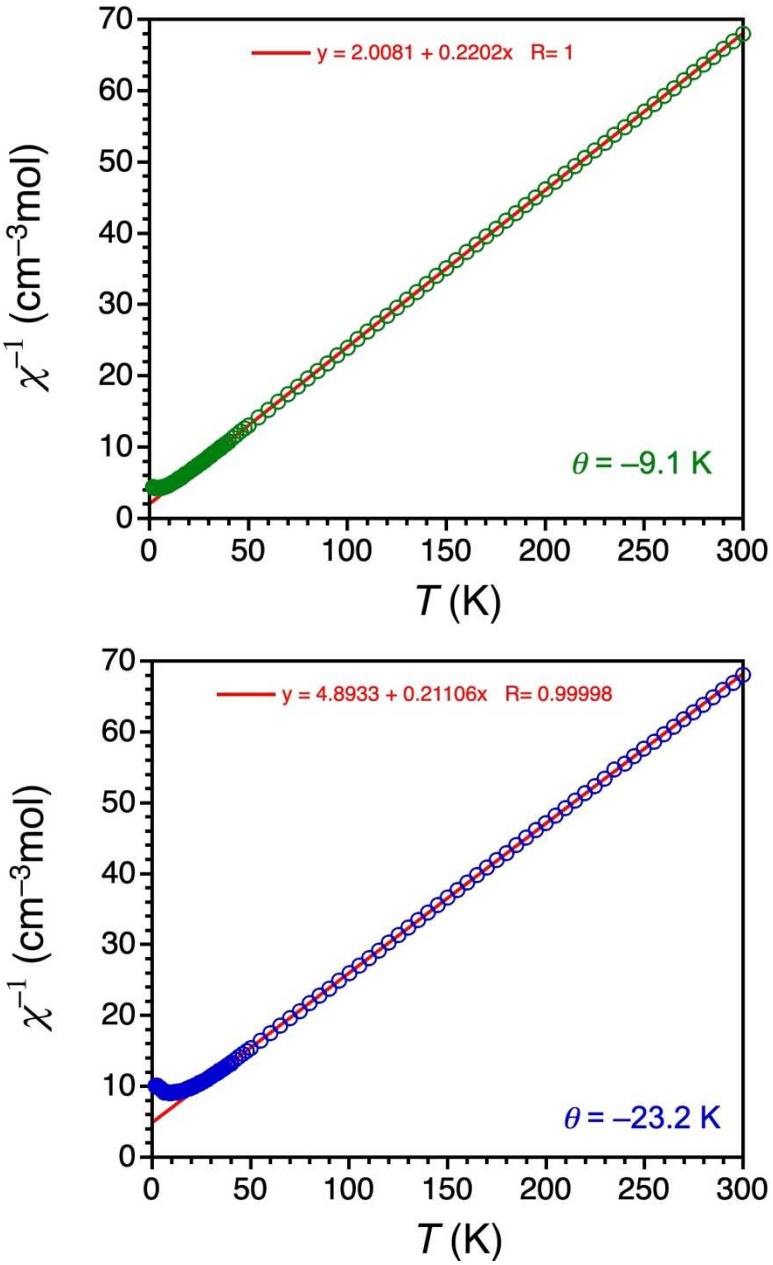

Fig. S13 Temperature dependence of χ^{-1} (where $\chi = M/H$ is the magnetic susceptibility normalized by mole of the formula unit, Table S1) measured at 0.1 T for the $FeCl_4^-$ (in green circles, upper) and $FeBr_4^-$ (in blue circles, lower) salts. The solid red lines are the best fits of the experimental data between 50 and 300 K to the Curie-Weiss law.

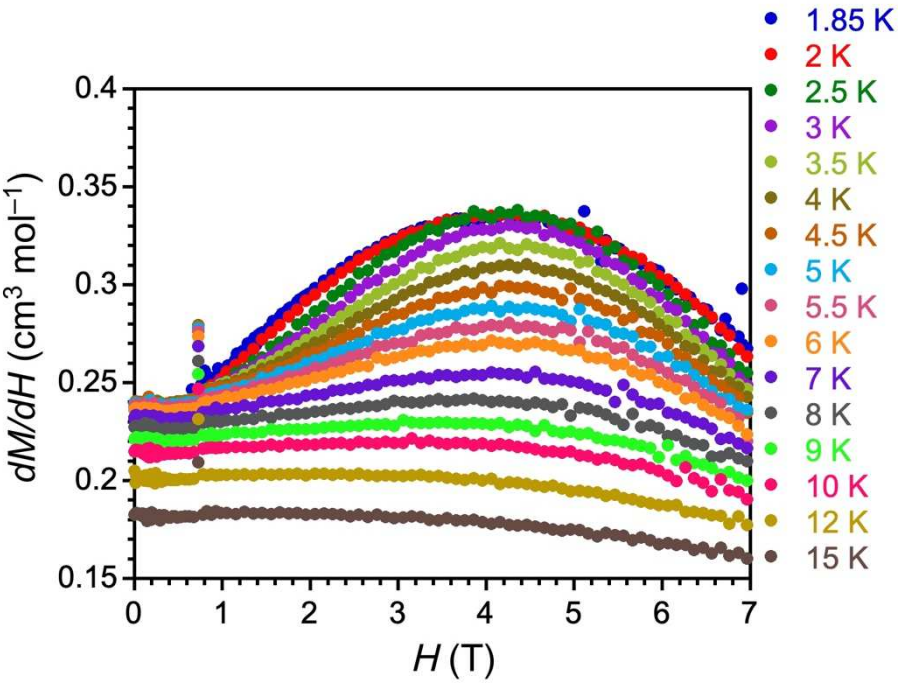

Fig. S14 Plot of first derivative of *M* vs *H* for a polycrystalline sample of the $FeCl_4^-$ salt as a function of applied field up to 7 T between 1.85 and 15 K.

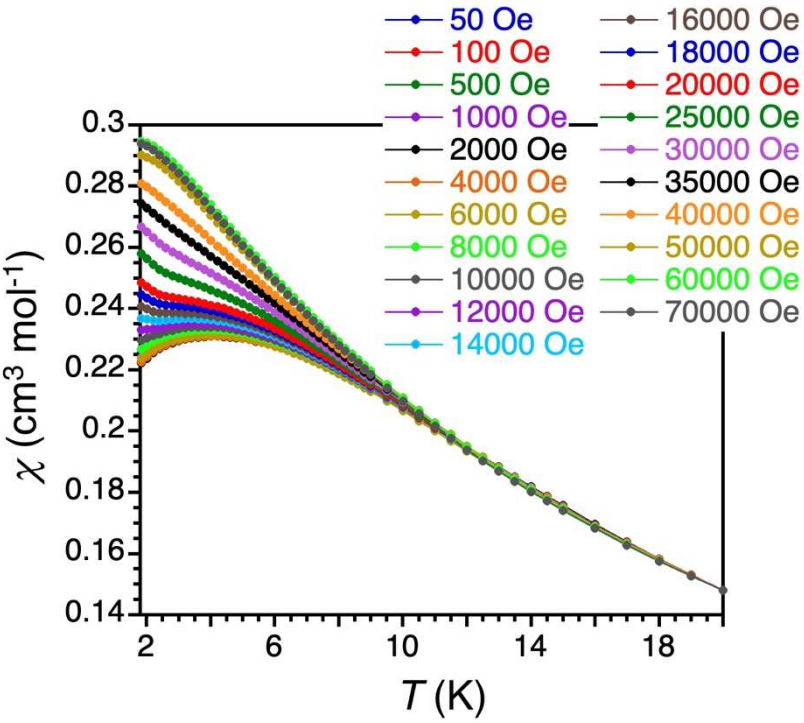

Fig. S15 Temperature dependence of the molar magnetic susceptibility (χ) for a polycrystalline sample of the $FeCl_4^-$ salt at different dc fields up to 7 T. Solid lines are guides for the eye.

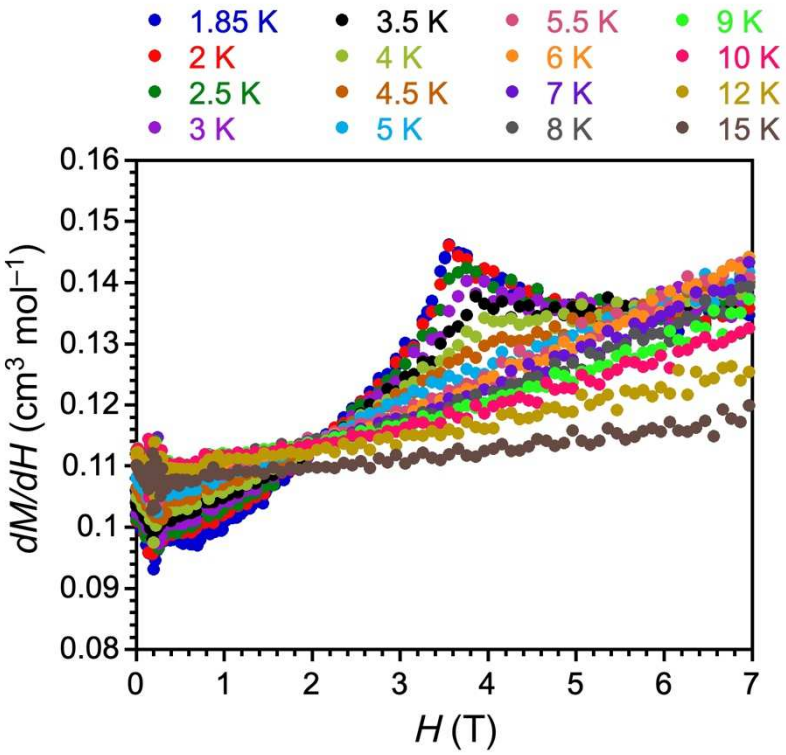

Fig. S16 Plot of first derivative of *M* vs *H* for a polycrystalline sample of the $FeBr_4^-$ salt as a function of applied field between 1.85 and 15 K.

G) Magneto-structural correlation

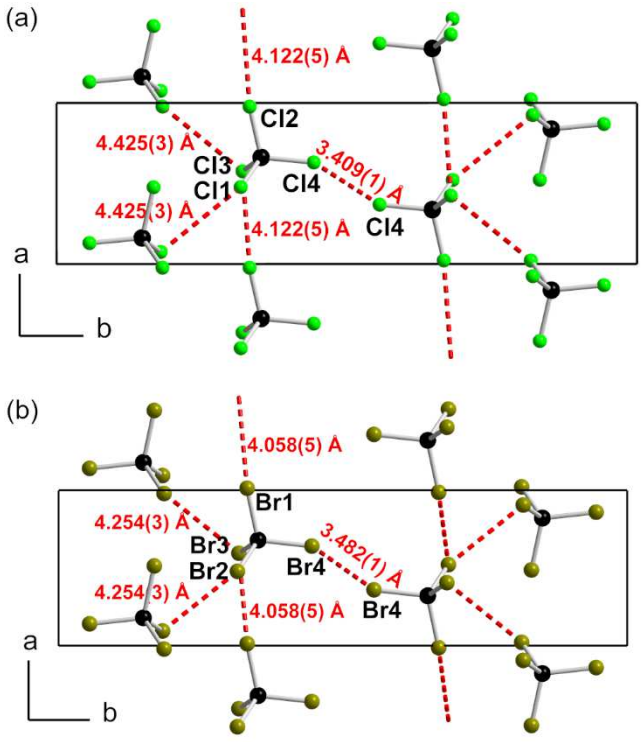

Fig. S17 Compared halogen•••halogen interactions in (a) (**1**)$FeCl_4$ and (b) (**1**)$FeBr_4$.

H) Thermodynamic properties

Heat capacity was measured by the thermal relaxation technique using a Quantum Design Physical Property Measurement System (PPMS-9) on pressed pellets of (**1**)($FeCl_4$) (1.44 mg), and (**1**)($FeBr_4$) (2.14 mg), which were molded under a pressure of 2 tons for 5 minutes. Measurements were performed on these compounds in zero-*dc* field between 298 and 2 K using Apiezon N grease for thermal contact. A small amount of Apiezon N grease (0.7 mg) was measured independently to estimate the sample environment correction, which was then subtracted from the total heat capacity of the sample.

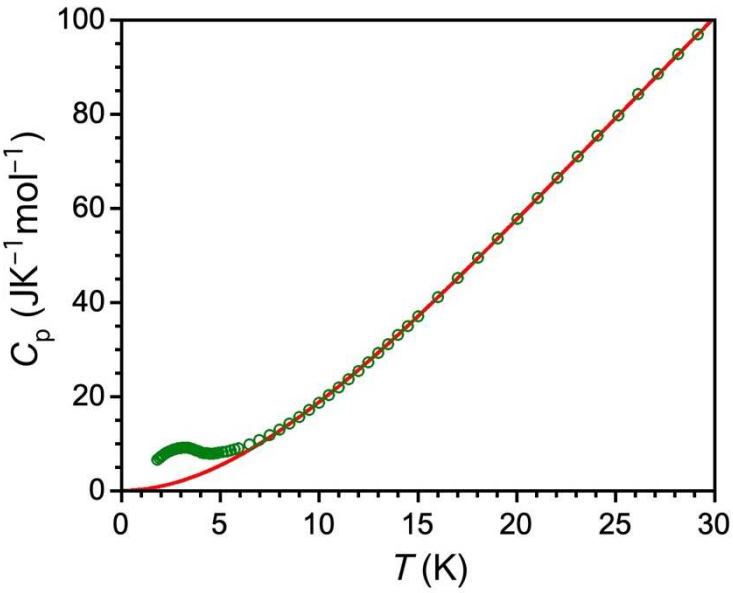

Fig. S18 Temperature dependence of the heat capacity, C_p, per mole of the $FeCl_4^-$ salt measured on a polycrystalline sample under zero applied field. The red solid line corresponds to the empirical polynomial base line used to determine the non-magnetic background of the heat capacity ($C_{p,background}$).

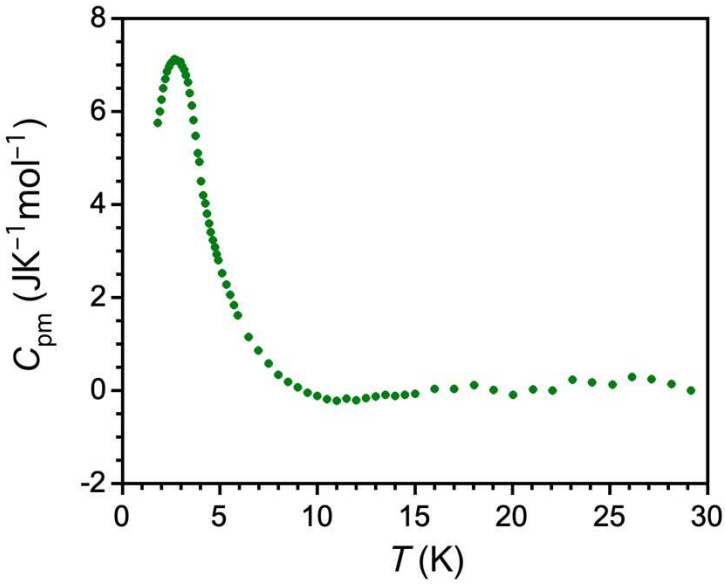

Fig. S19 Temperature dependence of the magnetic component (C_{pm}) of the heat capacity of the $FeCl_4^-$ salt deduced from $C_{pm} = C_p - C_{p,background}$.

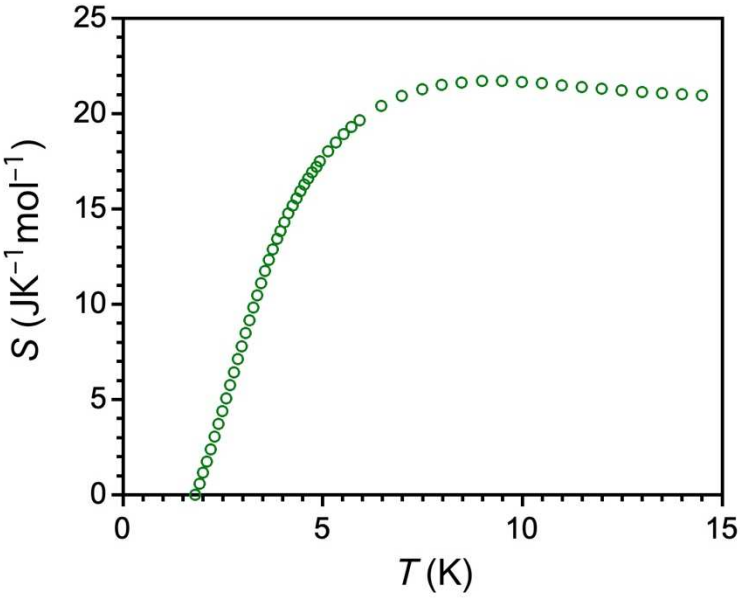

Fig. S20 Temperature dependence of the magnetic entropy, S, deduced from the numerical integration of C_{pm}/T per mole of the $FeCl_4^-$ salt measured on a polycrystalline sample under zero-applied field.

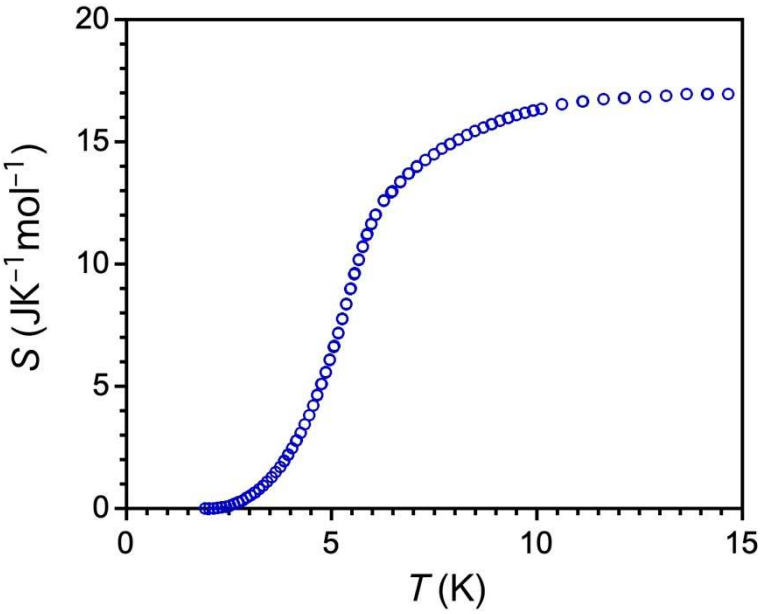

Fig. S21 Temperature dependence of the magnetic entropy, *S*, deduced from the numerical integration of C_{pm}/T per mole of the $FeBr_4^-$ salt measured on a polycrystalline sample under zero-applied field.

I) Powder diffraction diagrams

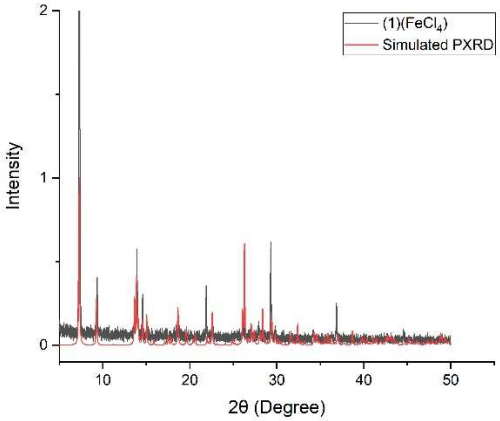

Fig. S22 X-ray powder diagram of a polycrystalline sample of (**1**)$FeCl_4$ performed at 298K, with simulated diagram deduced from single-crystal diffraction performed at 150 K.

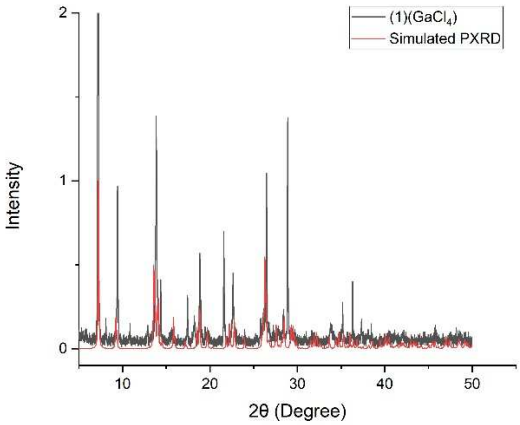

Fig. S23 X-ray powder diagram of a polycrystalline sample of (**1**)$GaCl_4$ performed at 298K, with simulated diagram deduced from single-crystal diffraction performed at 150 K.

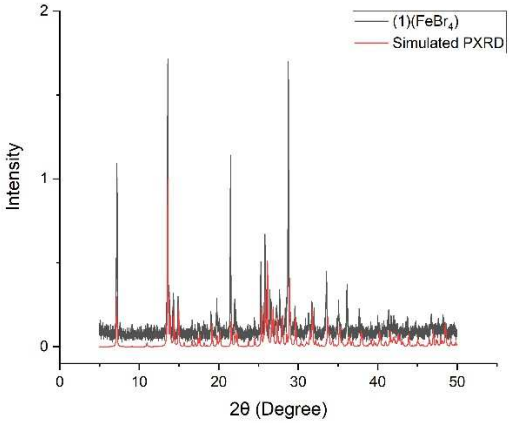

Fig. S24 X-ray powder diagram of a polycrystalline sample of (**1**)$FeBr_4$ performed at 298K, with simulated diagram deduced from single-crystal diffraction performed at 150 K.

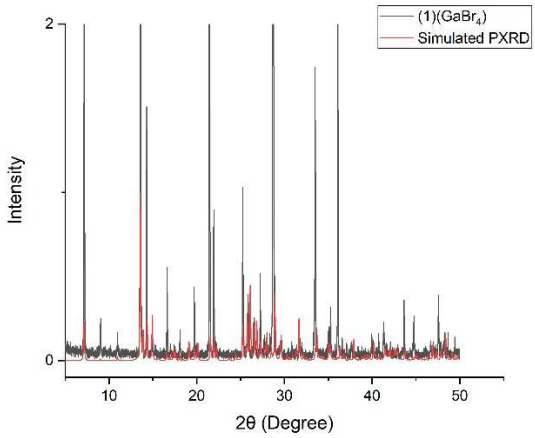

Fig. S25 X-ray powder diagram of a polycrystalline sample of (**1**)$GaBr_4$ performed at 298K, with simulated diagram deduced from single-crystal diffraction performed at 150 K.

References

[1] (a) D. J. Press and T. G. Back, *Org. Lett*., 2011, **13**, 4104–4107; (b) D. J. Press, T. G. Back and T. C Sutherland, *Tetrahedron Lett.,* 2012, **53**, 1603–1605.

[2] P. A Shapley, W. S. Bigham and M. T. Hay, *Inorg. Chim. Acta,* 2003, **345**, 255–260.

[3] A. Miyazaki, H. Yamazaki, M. Aimatsu, T. Enoki, R. Watanabe, E. Ogura, Y. Kuwatani, and M. Iyoda, *Inorg Chem.,* 2007, **16**, 3353–3366.

[4] G. M. Sheldrick, *Acta Cryst*., 2015, **A71**, 3.

[5] G. M. Sheldrick, *Acta Cryst*., 2015, **C71**, 3.

[6] L. J. Farrugia, *J. Appl. Cryst*., 2012, **45**, 849.

[7] C. Figliola, L. Male, P. N. Horton, M. B. Pitak, S. J. Coles, S. L. Horswell and R. S. Grainger, *Organometallics,* 2014, **33**, 4449–4460.